Received: 30 June 2021 | Revised: 30 August 2021 | Accepted: 30 August 2021

DOI: 10.1002/eqe.3546

RESEARCH ARTICLE

WILEY

Seismic reliability implied by behavior-factor-based design

Georgios Baltzopoulos | **Antonio Grella** | **Iunio Iervolino**

Dipartimento di Strutture per l'Ingegneria e l'Architettura, Università degli Studi di Napoli Federico II, Naples, Italy

Correspondence
Iunio Iervolino, Dipartimento di Strutture per l'Ingegneria e l'Architettura, Università degli Studi di Napoli Federico II, Via Claudio 21, 80125, Naples, Italy.
Email: iunio.iervolino@unina.it

Abstract

Force-based seismic design involves the reduction of elastic spectra by introducing a behavior factor, q. This approach is widespread in engineering practice; however, recent studies have shown that structures consistently designed at different sites will not share the same level of seismic risk, which can be defined as the annual rate of the structure failing to meet a seismic performance objective, despite seismic actions having the same exceedance return period at all sites. This paper investigates whether the definition of site-specific q factors can lead to uniform risk across sites characterized by varying levels of seismic hazard, based on the pushover curves of bare frame reinforced concrete buildings. These pushover curves are used to establish the backbones of equivalent single degree of freedom systems with varying lateral resistance. These systems are fictitiously placed at several Italian sites and their seismic failure risk is computed by integrating their fragility, assessed by means of incremental dynamic analysis, with each site's hazard curve. By assuming an arbitrary risk threshold, the same for all sites, the corresponding lateral strength leading to said threshold is determined and the corresponding behavior factor is back calculated. As expected, risk-targeted q factors tend to increase with decreasing seismic hazard and are highly sensitive to the shape of the hazard curve beyond the design return period. Coupled with the fact that at low hazard sites lateral strength is determined by detailing for gravity-load design and minimum code requirements, rather than seismic design actions, the results suggest that q factor-based design is unsuitable for warranting territorially uniform seismic safety, yet it may be suitable for setting an upper-bound to the annual failure probability.

KEYWORDS
performance-based seismic design, q factor, risk, safety, seismic fragility, seismic hazard

1 | INTRODUCTION

Modern seismic codes, such as Eurocode 8 (EC8)[1] and the current Italian code (NTC18),[2] require structures to be designed to meet certain seismic performance objectives, identified by limit states, for some corresponding design actions. The latter are defined by means of elastic pseudo-acceleration response spectra whose ordinates, taken individually, have the

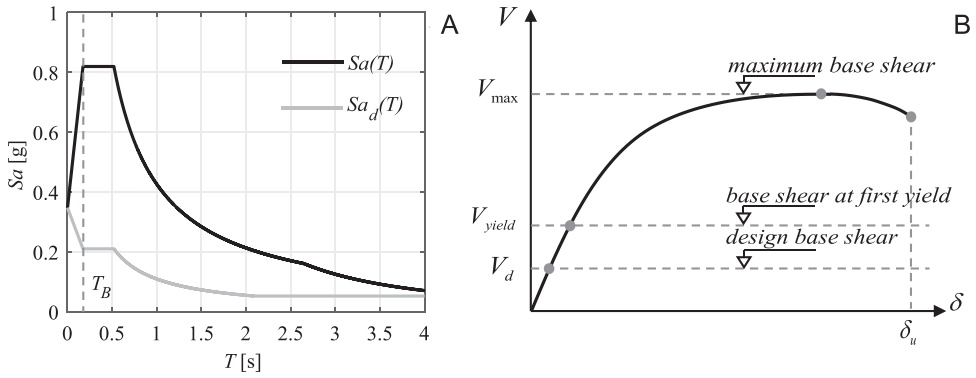

FIGURE 1 (A) Reduction of a horizontal elastic spectrum via q factor to obtain horizontal design spectrum (the design spectrum was constructed according to the provisions of the Italian code NTC18; the EC8 design spectrum would differ in the $T < T_B$ segment, but this is not relevant for the present study, as all structural vibration periods considered fall beyond T_B, that is in the zone where the definitions of NTC18 and EC8 design spectra coincide); (B) graphical representation of overstrenght on a static pushover curve

same exceedance return period (T_R) at the site of interest; i.e., by *uniform-hazard* spectra. Design of ordinary building structures covered by the codes is often driven by a *force-based* verification against the *life-safety* limit state, which is typically performed considering seismic actions with $T_R = 475$ years. The performance objective for the structure against that level of ground shaking is to dissipate seismic energy via inelastic excursions of structural members, while retaining its structural integrity and sufficient bearing capacity against gravity loads. To this aim, the force-based design philosophy assigns strength to the various structural elements according to force demands calculated via linear-elastic analysis, for example modal response analysis, using spectral ordinates that have been reduced (Sa_d) by means of a so-called *behavior factor*, or q factor, by a margin that depends on the vibration period T, as shown in Figure 1A.

The reasoning behind reducing the design actions by means of the q factor, is to allow structural elements to yield under the design ground motion to trigger hysteretic dissipation. Current European standards, such as EC8 and NTC18, prescribe a maximum allowable behavior factor, $q_{\max}$, to be applied to all structures of a specific building typology or class, that is to buildings sharing the same primary building material(s) and structural system adopted for resisting horizontal actions. This maximum allowable value of the behavior factor is known to depend on the deformation and dissipative capacity of the lateral-load-resisting system and on the, so-called, *overstrength* that said system exhibits. These concepts are illustrated in Figure 1B, which plots the static pushover (SPO) curve of a generic building structure. In the figure, the ordinate shows the resultant of monotonically increasing lateral forces acting on the building, that is base shear V, and the abscissa registers the roof-level lateral displacement δ caused by these forces. The SPO curve is indicatively shown to end at an ultimate displacement δ_u, representing an admissible deformation that can be reached without compromising gravity-load bearing capacity. The figure also highlights that the base shear causing the first cross-section to reach yield, V_{yield}, and the maximum base shear the building can sustain prior to the onset of strength deterioration under monotonic loading, $V_{\max}$, exceed the demand resulting from elastic analysis, V_d. In other words, the actions that will actually force the structure to exhibit inelastic deformations are higher than the design actions, for reasons related to section-level design, reinforcement detailing and the system's capacity for redistribution of internal forces.[3]

Assuming, for the time being, that overstrength and deformation capacity can be considered invariant among buildings of the same typology, it can be postulated that having the different buildings belonging to that typology share a common code-prescribed $q_{\max}$, stems from the implied expectation that this should lead to uniformity of seismic reliability (i.e., *seismic risk*) of these structures. On the other hand, the Italian national-level research program *Rischio Implicito – Norme Tecniche per le Costruzioni* (RINTC;[4] the risk implicit in the technical code for construction—translated from Italian) sought to analytically quantify seismic risk of code-conforming building structures by computing the *annual failure rate*, that is the annual occurrence rate of earthquakes that cause failure of the structure to meet a predefined seismic performance objective. That work led to the conclusion that similar buildings designed using the same behavior factor at different sites, can turn out to exhibit different levels of seismic risk,[4] which was also corroborated by other studies.[5–8] In fact, it was observed that the seismic risk for newly-designed buildings increases with increasing seismic hazard at the site, even though the design actions increase commensurately with any increase in hazard.

The results of the RINTC project constitute the foundations of the present study, which investigates the possibility of calculating site-dependent risk-targeted q factors for some typical building structures. The designation *risk-targeted q factors*, is used here in the sense that the reduction in elastic lateral strength demand V_d is to be calibrated to provide uniform

seismic risk across a variety of considered building sites, as proposed by other researchers in the past.[5,8–10] The present investigation is based on the pushover curves of selected reinforced concrete (RC) frame buildings that were designed, modelled, and analyzed within the activities of the aforementioned research project RINTC. The static pushovers of these RC frames, which had been designed against different seismic hazard levels at various sites, are used to establish the backbone curves and dynamic characteristics of equivalent single degree of freedom (ESDoF) systems.[11] Furthermore, by interpolating among these backbones, which exhibit varying levels of lateral resistance according to the hazard at the site for which they were designed, additional SDoF oscillators are defined, to obtain a family of simple (idealized) structures with an almost continuous variation of lateral strength (e.g., in terms of $V_{\max}$), and whose characteristics can be held to be representative of the building typology of the original designs. These ESDoF systems are then subjected to incremental dynamic analysis (IDA),[12] in order to analytically procure their fragility curves for a selected performance objective. Subsequently, each set of SDoF oscillators is fictitiously placed at various Italian sites, each characterized by a different hazard curve, and their annual failure rates are evaluated. By assigning an (arbitrary) seismic risk target, the lateral strength level, necessary to meet that risk criterion, is established per site. Finally, the contribution of overstrength is considered in order to back-calculate the necessary q factor that would have led to that specific design. This study, although applying the Italian code, could attract international interest given the similarities with other international codes, most notably EC8.

This study is discussed in the remainder of this article, which is structured as follows: first, an overview of the methodology used for obtaining the necessary computational tools is provided, including a description of the case study buildings, the use of pushover analyses to define equivalent SDoF models, fragility analysis and probabilistic seismic hazard analysis for each site considered. Then, the assumptions and method for determining risk-targeted behavior factors for each case are presented, followed by a presentation and discussion of the results. The conclusions of this study are summarized in the final section.

2 | METHODOLOGY

2.1 | Reliability assessment

For the purposes of the present investigation, the seismic safety of structures is quantified in terms of their annual failure rate, λ_f. According to the *performance-based earthquake engineering* paradigm (PBEE),[13] λ_f can be computed via Equation (1):

$$\lambda_f = \int_{IM} P\left[f \,|IM = im\right] \cdot \left|d\lambda_{im}\right|, \tag{1}$$

where $P[f|IM = im]$ denotes the probability of failure of a specific performance objective, given that some ground motion intensity measure (IM) takes a specific value, im, and λ_{im} is a measure of seismic hazard at the construction site, defined as the annual rate of earthquakes exceeding that value of shaking intensity. The terms typically used in PBEE for $P[f|IM = im]$ and λ_{im} are the structure's *fragility function* and the site's *hazard curve*. At the state-of-art of seismic risk studies, analytical estimation of fragility functions is performed by conducting a series of nonlinear dynamic analyses on a numerical model of the structure, while λ_{im} is obtained by means of a probabilistic seismic hazard analysis (PSHA).[14,15]

2.2 | Case-study structures

The case-study structures used in this investigation were chosen among the buildings designed, modelled and analyzed within the activities of the RINTC-project. More specifically, six RC bare frames are considered, that is three-, and six-storey RC moment-resisting frame structures, regular in plan and elevation, that were designed according to the Italian NTC18 code at three Italian sites, namely L'Aquila, Naples, and Milan. Each of these sites is representative of a different design level of seismic hazard, with L'Aquila being the highest-hazard site of the three and Milan the lowest. All buildings are destined for residential use and share the same basic layout in plan, shown in Figure 2, with first-storey height of 3.40 m and 3.05 m for the remaining storeys. Each structure was designed against gravity and seismic loads, for the latter via modal response spectrum analysis using a behavior factor q equal to 3.90 and assuming soil class C, according to NTC18 classification (the same as EC8). As a consequence, buildings with the same height but designed against the seismic actions

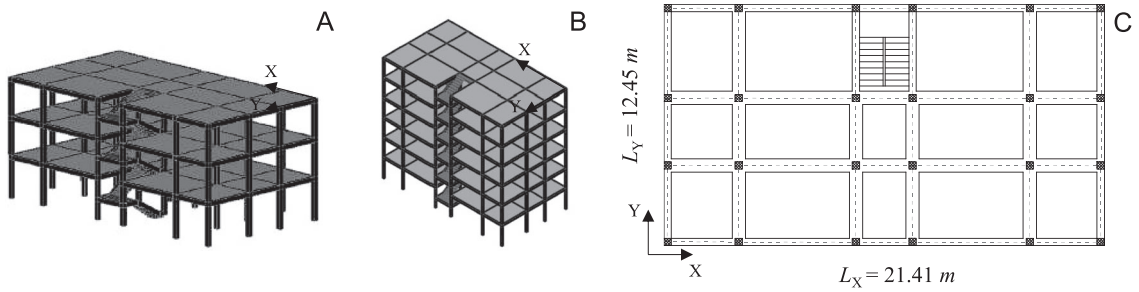

FIGURE 2 View of the structural elements of the case-study RC frames and designation of the two principal directions X and Y: (A) three-storey frame; (B) six-storey frame; (C) layout of structural elements in plan, common to both RC frames (L_X, L_Y represent the lenghts of each side of the building)

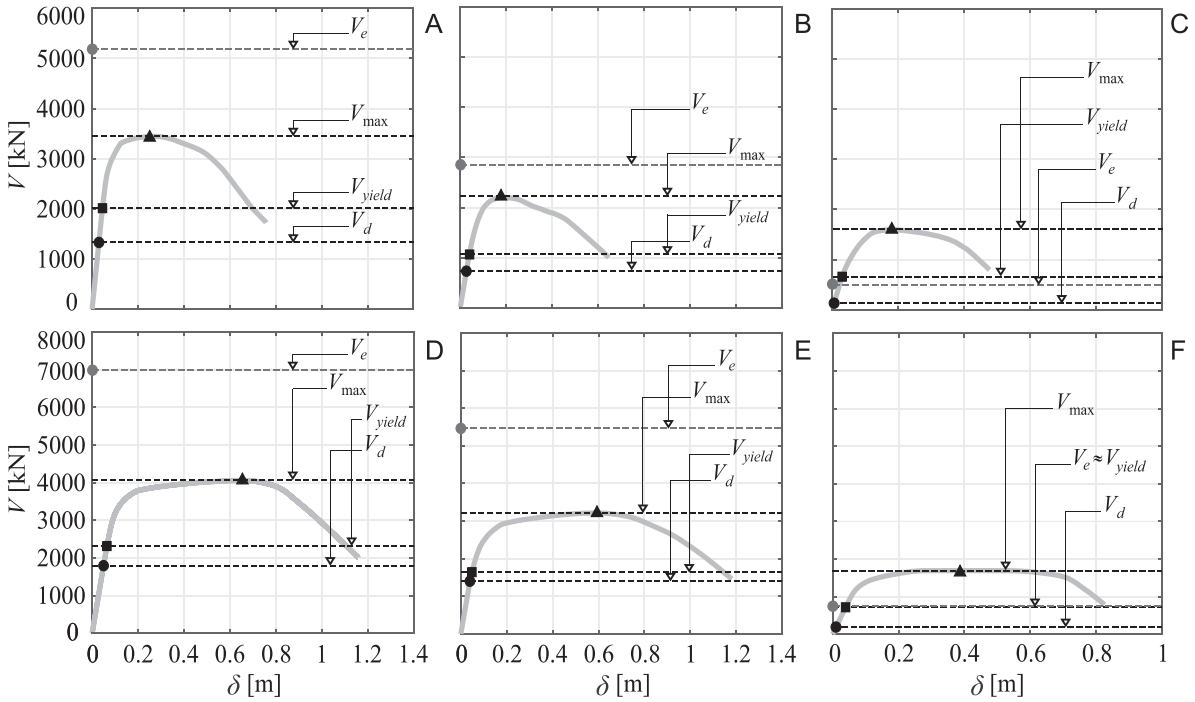

FIGURE 3 Pushover curves of the case-study structures; (A) 3-storey building in L'Aquila, Y direction; (B) 3-storey building in Naples, Y direction; (C) three-storey building in Milan, Y direction; (D) six-storey building in L'Aquila, X direction; (E) six-storey building in Naples, X direction; (F) six-storey building in Milan, X direction

of different sites, only differ in the dimensions and reinforcement detailing of structural elements, while their overall configuration is the same. Details on the design and modelling of these buildings can be found in dedicated literature.[16]

2.3 | Structural models and ESDoF systems

As part of the activities of the RINTC project, two separate numerical models were developed for each one of these buildings: an elastic model used for modal response analysis during code-based design and a more refined lumped-plasticity model.[17] The reason behind dual modelling was that the former was intended to replicate standard engineering design practice, while the latter followed the state-of-the-art in modelling the post-yield hysteretic behavior of RC members and was used for conducting static non-linear analyses in the two principal directions of each building, arbitrarily designated X and Y. Some of the six buildings' SPOs can be seen in Figure 3, where the previously mentioned characteristic points, defined by V_d, V_{yield}, V_{max} and nominal elastic base shear demand V_e, are marked against each curve along with their corresponding roof displacements. Each pushover curve is plotted up to the point corresponding to a fifty percent drop

TABLE 1 Design parameters for the case-study structures used in this investigation

Site	three-storey, X direction				three-storey, Y direction				six-storey, X direction				six-storey, Y direction			
	T_1 [s]	$\tilde{m}_1$ [t]	V_e [kN]	V_d [kN]	T_1 [s]	$\tilde{m}_1$ [t]	V_e [kN]	V_d [kN]	T_1 [s]	$\tilde{m}_1$ [t]	V_e [kN]	V_d [kN]	T_1 [s]	$\tilde{m}_1$ [t]	V_e [kN]	V_d [kN]
L'Aquila	0.44	613	4925	1263	0.46	645	5184	1329	0.90	1506	6992	1793	0.79	1487	7863	2016
Naples	0.62	581	2728	699	0.63	618	2854	732	0.88	1654	5466	1401	0.80	1674	6085	1560
Milan	0.86	641	653	167	0.74	432	511	131	1.66	1413	745	191	1.42	1563	964	247

in lateral resistance, which was used within the RINTC project to define the collapse threshold in terms of displacement response. The pushover curves of these buildings form the starting point of the analyses described in the remainder of the article.

Design base shear per principal direction V_d is determined via spectral modal response analysis of the linear-elastic model used for design.[18] Strictly speaking, this modal analysis entails multiple-mode contribution to base shear; however, given that all structures considered are first-mode dominated in both directions, with primarily translational modes, for the purposes of the present study the simplification is made to only consider the first mode contribution, according to Equation (2):

$$V_d = \tilde{m}_1 \cdot Sa_d(T_1), \tag{2}$$

where T_1 is the fundamental period of vibration resulting from the numerical model used for design purposes, $Sa_d(T_1)$ is the design spectral acceleration at that period and $\tilde{m}_1$ is the associated participating modal mass, also calculated from the elastic model used for design (see Figure 1A). According to the Italian code NTC18, design spectral acceleration $Sa_d(T)$ is in turn given, as a function of the q factor, by Equation (3):

$$\begin{cases} Sa_d(T) = Sa(0) + \frac{T}{T_B} \cdot \left[\frac{Sa(T_B)}{q} - Sa(0)\right], 0 \le T < T_B \\ Sa_d(T) = \frac{Sa(T)}{q}, T \ge T_B \end{cases}, \tag{3}$$

where $Sa(T)$ are the elastic horizontal pseudo-acceleration spectral ordinates of the code at vibration period T, T_B is the period marking the beginning of the constant-acceleration branch of the code spectrum and $Sa(0)$, $Sa(T_B)$ are the elastic spectral ordinates at $T = 0$s (i.e., the peak ground acceleration) and $T = T_B$, respectively. Analogously, the nominal elastic base shear demand, V_e, can be obtained via Equation (4):

$$V_e = \tilde{m}_1 \cdot Sa(T_1). \tag{4}$$

These design-related parameters for the six case-study structures considered, specifically T_1, $\tilde{m}_1$, V_e and V_e, are provided in Table 1.

2.4 | Reference ESDoF systems

For the purposes of the present study, twelve reference equivalent SDoF oscillators were defined using these SPO curves, one for each structure's two principal directions.[11] Examination of each direction separately is justified by the buildings' regularity in plan, which precludes torsional effects dominating seismic response. The transition from a multiple DoF (n-story) building to an ESDoF system is schematically presented in Figure 4. Each MDoF structure's SPO curve was converted to a so-called capacity curve of the ESDoF system by dividing both base shear and roof displacement with the first-mode modal participation factor Γ.[19] The resisting force and displacement of the ESDoF oscillator are denoted as $F^* = V/\Gamma$ and $\delta^* = \delta/\Gamma$, respectively. Subsequently, each ESDoF's backbone curve is approximated via a tri-linear function, defined by five parameters, as shown in Figure 4C: the nominal yield force and displacement, F_y^* and δ_y^* respectively, the capping-point force and displacement, F_c^* and δ_c^*, and the ultimate displacement, δ_u^*, which corresponds to complete loss of strength. The tri-linear approximation to the capacity curve follows the procedure implemented

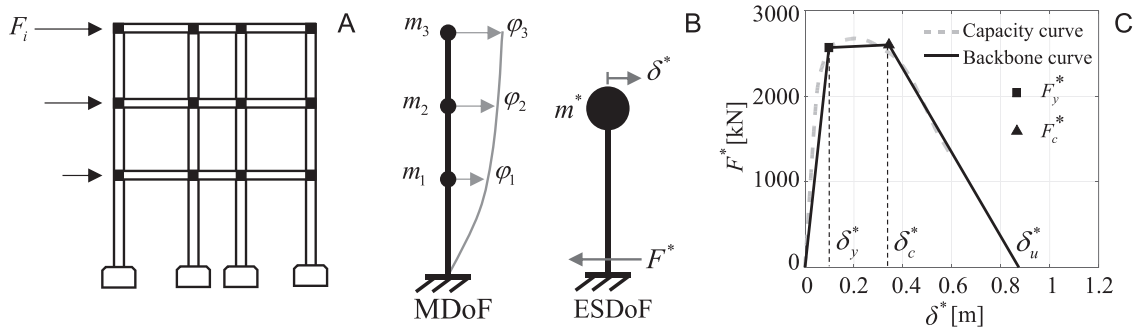

FIGURE 4 Schematic representation of pushover-based conversion of the building into an ESDoF oscillator; (A) pushover analysis of the lumped mass MDoF structural model per direction; (B) mass, displacement and restoring force of the ESDoF system; (C) tri-linear backbone approximation of the capacity curve in the Y direction of the three-storey building designed for L'Aquila

TABLE 2 Parameters of the reference ESDoF oscillators

Site	three-storey, X direction								three-storey, Y direction							
	m^* [t]	T^* [s]	Γ [-]	F_y^* [kN]	F_c^* [kN]	δ_y^* [m]	δ_c^* [m]	δ_u^* [m]	m^* [t]	T^* [s]	Γ [-]	F_y^* [kN]	F_c^* [kN]	δ_y^* [m]	δ_c^* [m]	δ_u^* [m]
L'Aquila	534	0.86	1.30	2586	2614	0.092	0.421	0.936	543	0.90	1.29	2572	2604	0.098	0.343	0.874
Naples	496	1.13	1.29	1501	1513	0.098	0.371	0.736	510	1.12	1.28	1672	1675	0.104	0.290	0.705
Milan	497	1.31	1.28	1191	1194	0.105	0.346	0.664	508	1.29	1.27	1217	1226	0.101	0.261	0.503
Site	**six-storey, X direction**								**six-storey, Y direction**							
	m^* [t]	T^* [s]	Γ [-]	F_y^* [kN]	F_c^* [kN]	δ_y^* [m]	δ_c^* [m]	δ_u^* [m]	m^* [t]	T^* [s]	Γ [-]	F_y^* [kN]	F_c^* [kN]	δ_y^* [m]	δ_c^* [m]	δ_u^* [m]
L'Aquila	1177	1.49	1.31	2839	3088	0.135	0.609	1.174	1147	1.15	1.33	3874	3942	0.113	0.510	1.058
Naples	1306	1.74	1.29	2247	2483	0.133	0.597	1.208	1376	1.66	1.26	2584	2739	0.131	0.525	1.041
Milan	1245	2.25	1.28	1210	1291	0.125	0.543	0.748	1283	2.28	1.26	1502	1537	0.154	0.507	0.693

in previous applications,[20] based on a dedicated study,[21] with the exception that δ_y^* is deliberately set at the point corresponding to the formation of a plastic mechanism for each frame, which results in the ESDoF systems having nominal yield points that correspond to similar roof drifts.

The equivalent mass of each ESDoF is calculated[19] as $m^* = \sum_{i=1}^{k} m_i \cdot \varphi_i$, where m_i and φ_i with $i = \{1, 2, \ldots, k\}$ are, respectively, the i-th floor mass and corresponding component of the first modal vector. In this context, the modal vector is normalized to have unit value at roof level and the vibration period of the ESDoF oscillator can be calculated as per Equation (5):

$$T^* = 2\pi \cdot \sqrt{m^* \cdot \delta_y^* / F_y^*}. \tag{5}$$

These parameters are reported for each of the twelve reference ESDoF systems in Table 2.

2.5 | Generated ESDoF systems

The reference ESDoF oscillators presented in the preceding paragraph correspond to RC frames of the same configuration, but designed for sites in Milan, Naples and L'Aquila, listed here in ascending order of seismic design actions for the considered (life-safety) limit state. Therefore, each triplet of ESDoF systems represents variations of approximately the same structure, but designed to exhibit different lateral-force-resisting capacity by varying cross-section sizes and reinforcement detailing. For the purposes of this study, additional ESDoF oscillators were generated by linearly interpolating between the characteristic force-displacement points F_y^*, δ_y^*, F_c^*, δ_c^* and δ_u^* of the reference ESDoF oscillators. These new

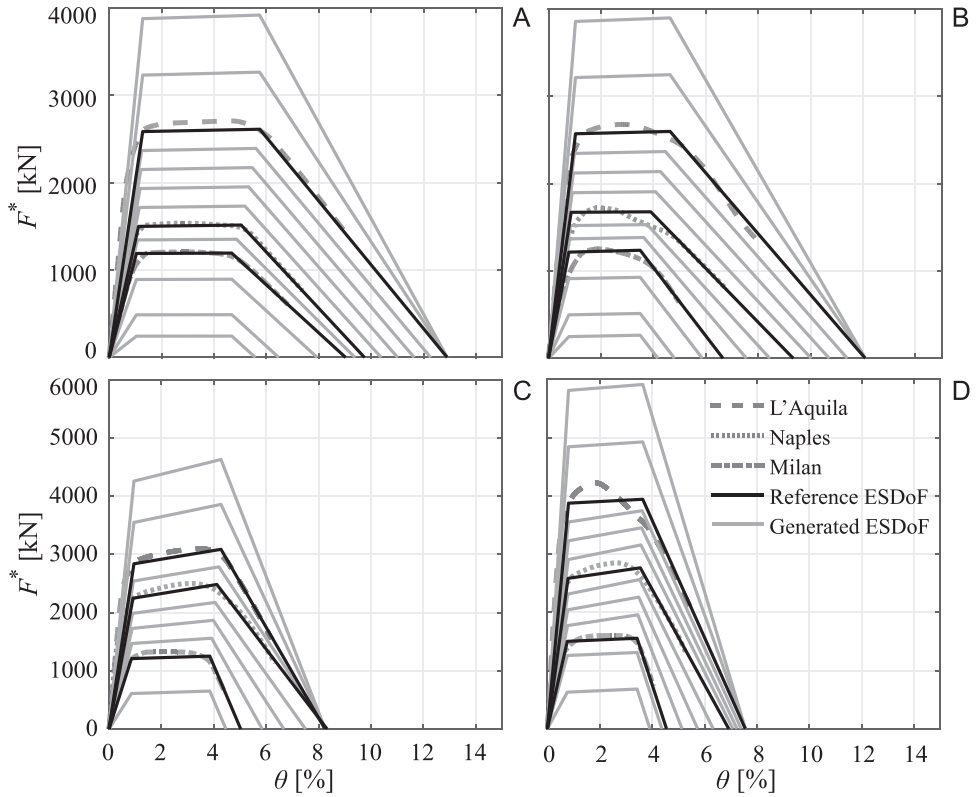

FIGURE 5 Definition of additional backbone curves via interpolation of the backbones of (A) the three-storey building, in the X direction; (B) the three-storey building, in the Y direction; (C) the six-storey building, in the X direction; (D) the six-storey building, in the Y direction

backbones are shown in Figure 5, where the backbone curves of the ESDoF oscillators corresponding to structures that resulted from actual design are plotted in black lines.

In the abscissa the roof displacement has been normalized with respect to each building's height, H, thus reporting roof drift ratio $\theta = \Gamma \cdot \delta^*/H$. It can be observed that nominal yield points for all structures are around $\theta = 1\%$, which is a drift around which a global plastic mechanism is expected to form for RC structures.[22,23] The equivalent masses assigned to each of these generated oscillators are also the result of linear interpolation between the m^* values of the reference models and thus the vibration period T^* of each generated SDoF oscillator can be calculated via Equation (5). It is convenient to express the lateral resisting capacity of these systems using a dimensionless parameter termed the yield strength coefficient, C_y, defined as the ratio of spectral acceleration at the structure's vibration period causing yield, $Sa_y(T^*)$, divided by the acceleration of gravity, according to Equation (6):

$$C_y = \frac{Sa_y(T^*)}{g} = \frac{\delta_y^*}{g} \cdot \left(\frac{2\pi}{T^*}\right)^2. \tag{6}$$

Figure 5 also shows that, for each building's principal direction, a number of backbones were also obtained from extrapolation beyond the lowest and highest lateral resistance cases (i.e., Milan and L'Aquila, respectively). However, for the two backbones generated above the ones corresponding to the L'Aquila designs, that is the reference systems with the highest lateral strength, δ_u^* was not extrapolated but held constant, to avoid adjudicating response in a region that will have no impact in the final results, as will become evident later on.

An overall summary of the yield strength coefficient C_y, the yield and capping-point displacements δ_y^*, δ_c^* and the vibration period T^* of these SDoF systems is provided in Table 3. The result of this exercise is four sets of SDoF systems with varying levels of lateral strength, which are considered to be approximately representative of variants of the original reference structures, as they would have ostensibly resulted from design against seismic actions of varying intensity. While the same premise cannot be made for the SDoF systems obtained via extrapolation to C_y values beyond the bounds of the

TABLE 3 Defining parameters of the generated ESDoF oscillators

three-storey, X direction				three-storey, Y direction				six-storey, X direction				six-storey, Y direction			
C_y [-]	T^* [s]	δ_y^* [m]	δ_c^* [m]	C_y [-]	T^* [s]	δ_y^* [m]	δ_c^* [m]	C_y [-]	T^* [s]	δ_y^* [m]	δ_c^* [m]	C_y [-]	T^* [s]	δ_y^* [m]	δ_c^* [m]
0.74	0.71	0.094	0.421	0.72	0.65	0.076	0.343	0.37	1.21	0.135	0.609	0.52	0.94	0.113	0.510
0.62	0.78	0.094	0.421	0.60	0.71	0.076	0.343	0.31	1.33	0.135	0.609	0.43	1.03	0.113	0.510
0.49	0.87	0.094	0.421	0.48	0.80	0.076	0.343	0.25	1.49	0.135	0.609	0.34	1.15	0.113	0.510
0.46	0.90	0.091	0.411	0.45	0.81	0.073	0.330	0.21	1.60	0.134	0.603	0.31	1.22	0.114	0.514
0.42	0.92	0.089	0.401	0.41	0.83	0.070	0.317	0.18	1.74	0.133	0.597	0.27	1.31	0.115	0.518
0.38	0.96	0.087	0.391	0.37	0.85	0.067	0.303	0.16	1.83	0.131	0.588	0.23	1.42	0.116	0.521
0.35	0.99	0.085	0.381	0.33	0.88	0.064	0.290	0.14	1.94	0.129	0.579	0.19	1.57	0.117	0.525
0.31	1.04	0.082	0.371	0.30	0.91	0.062	0.280	0.12	2.08	0.127	0.571	0.17	1.64	0.116	0.521
0.28	1.08	0.080	0.359	0.27	0.94	0.060	0.271	0.10	2.25	0.125	0.562	0.16	1.72	0.115	0.516
0.24	1.13	0.077	0.346	0.24	0.98	0.058	0.261	0.05	3.17	0.125	0.562	0.14	1.82	0.114	0.512
0.18	1.30	0.077	0.347	0.18	1.13	0.058	0.261	–	–	–	–	0.12	1.95	0.113	0.507
0.10	1.76	0.077	0.347	0.10	1.53	0.058	0.261	–	–	–	–	0.10	2.13	0.113	0.507
0.05	2.49	0.077	0.347	0.05	2.16	0.058	0.261	–	–	–	–	0.05	3.01	0.113	0.507

reference structures, these are useful for providing some visual continuity to the results that follow but have no bearing on the final conclusions.

2.6 | Fragility functions

Within this study, each structure is (arbitrarily) considered to have failed if $\delta^*_{\max} \geq \delta^*_c$, with $\delta^*_{\max}$ being the maximum (absolute value) transient displacement of each ESDoF oscillator undergoing base-acceleration. In other words, nominal failure is taken to occur whenever seismic displacement demand exceeds a threshold value coinciding with each backbone's capping-point displacement; note that this is not intended to be representative of collapse, but simply a possible performance objective for seismic design of a nonlinear structure. This corresponds to a displacement demand of around four-and-a-half times the nominal yield displacement, for all ESDoF systems concerned. Although more than one performance objective could have been considered for the quantification of seismic safety, the choice was made to contain the investigation within the limits of this single performance.

To calculate the associated seismic risk in terms of λ_f, fragility functions are needed; i.e., $P[f|IM = im] = P[\delta^*_{\max} \geq \delta^*_c|IM = im]$. These fragilities were evaluated analytically, using the, so-called, IM-based approach,[24] based on IDA of the SDoF oscillators. The IM-based approach uses the IDA curves and introduces a random variable that is the shaking intensity value causing failure, designated as IM_f. By assuming that IM_f is lognormally distributed, fragility can be expressed as per Equation (7):

$$\begin{cases} P\left[f\,|IM = im\right] = P\left[IM_f \leq im\right] = \Phi\left[\frac{\ln(im)-\eta}{\beta}\right] \\ \eta = \frac{1}{n}\cdot\sum_{j=1}^{n}\ln\left(im_{f,j}\right) \\ \beta = \sqrt{\frac{1}{n-1}\cdot\sum_{j=1}^{n}\left[\ln\left(im_{f,j}\right)-\eta\right]^2} \end{cases}, \tag{7}$$

where η and β are, respectively, the mean and standard deviation of the natural logarithm of IM_f, both estimated from a sample of structural responses provided by dynamic analysis, $\Phi(\cdot)$ denotes the standard Gaussian function, n is the number of acceleration records used in the IDA, and $im_{f,j}$ with $j = 1, 2, \ldots, n$ is the IM_f realization obtained from dynamic analysis with the j-th record.

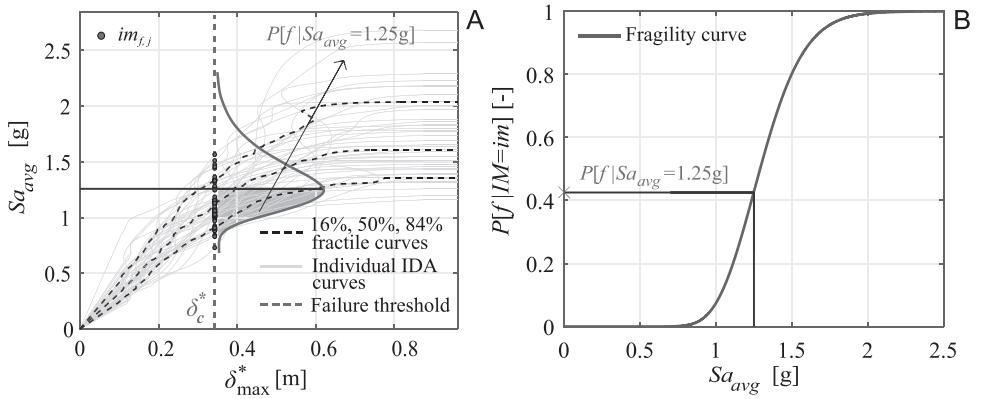

FIGURE 6 (A) IDA curves and IM_f sample at the failure threshold and (B) lognormal fragility curve fitted to the $im_{f,j}$ sample corresponding to a three-storey building's Y direction, with $C_y = 0.48$

The IM adopted in this study was an average spectral acceleration,[25] Sa_{avg}, defined as the geometric mean of 5% damped spectral accelerations at vibration periods T_i, $i = 1, 2, \ldots, k$, according to Equation (8):

$$Sa_{avg} = \left[\prod_{i=1}^{k} Sa\,(T_i)\right]^{1/k}. \tag{8}$$

In this case the following vibration periods T_i were selected for the definition of Sa_{avg}: $\{T_i\} = \{0.70, 0.75, 0.80, 0.85, 0.90, 0.95, 1.00, 1.10, 1.20, 1.30, 1.40, 1.50, 1.60, 1.70, 1.80, 1.90, 2.00\}$, with all values being in seconds. Past research has shown that such IMs are more *efficient* in predicting inelastic displacement response than single-spectral-ordinate IMs, by virtue of accounting for spectral shape beyond the structure's fundamental period.[26] This efficiency is quantified in terms of the dispersion of structural responses given various levels of the conditioning IM and has the practical result of limiting the amount of dynamic analyses required to obtain risk estimates within a target standard error.[27,28] In fact, this period interval contains almost all $T^*$of the generated ESDoF oscillators, bar a few with $C_y < 0.12$, and therefore Sa_{avg} could be a common IM to express the fragilities of all structures considered.[29] Finally, the so-called s*ufficiency* of $Sa_{avg}$with respect to the seismological parameters affecting hazard at each site,[30] implies that the same fragility functions can be exported to different sites.

IDA was conducted for each ESDoF oscillator using the DYANAS[31] interface for the OpenSees platform.[32] The modified Ibarra-Medina-Krawinkler peak-oriented hysteretic rule,[33] without cyclic degradation, was assigned to the oscillators for these analyses, along with five-percent-of-critical viscous damping. The forty-four acceleration records constituting the far-field FEMA-P695 set[34] were used in these analyses, which comprises accelerograms recorded on firm soil, compatible with the assumed ground type C, predominantly recorded during events in California, of magnitude range from 6.5 to 7.6 and distances between the site and the horizontal projection of the fault within the range from 11 to 27 kilometers.

The procedure used for defining each ESDoF's fragility function from the IDA results[35] is illustrated in Figure 6. The intersection of the j-th record's IDA curve with the vertical line $\delta^*_{max} = \delta^*_c$, provides one realization of the random variable IM_f, denoted as $im_{f,j}$ with $j = 1, 2, \ldots, 44$. The resulting fragility parameters for each ESDoF system, which are reported in Table 4, are then estimated based on this sample of IM_f realizations, according to Equation (7). The structure-specific fragility functions thus derived only account for one source of uncertainty, which is the so-called, *record-to-record variability* of structural response,[36] while uncertainty in the structural model is neglected, as previous RINTC-specific studies[37] supported to do so (it is worth observing that these fragility parameters are subject to estimation uncertainty, by virtue of being derived from samples of non-linear responses,[38] and this estimation uncertainty carries over to the calculated failure rates; even though this aspect is not treated here for the sake of brevity, it does not alter the results of the comparisons).

The fragility parameters are plotted in Figure 7 against the corresponding ESDoF oscillators' yield strength coefficients C_y, for one of the principal directions of the three-storey and six-storey configurations. The figure displays continuous functions of C_y that are fitted to the fragility parameters $\{\eta, \beta\}$ of each structural configuration (as will be discussed further on, this operation allows to calculate failure rates for any level of lateral resistance within a given range of site's design hazard covered by the continuous functions).

TABLE 4 Fragility parameters

three-storey, X direction			three-storey, Y direction			six-storey, X direction			six-storey, Y direction		
C_y [-]	e^{η} [g]	β [-]	C_y [-]	e^{η} [g]	β [-]	C_y [-]	e^{η} [g]	β [-]	C_y [-]	e^{η} [g]	β [-]
0.74	1.756	0.174	0.72	1.545	0.175	0.37	1.655	0.274	0.52	1.694	0.219
0.62	1.627	0.173	0.60	1.429	0.173	0.31	1.605	0.295	0.43	1.548	0.237
0.49	1.499	0.200	0.48	1.291	0.177	0.25	1.551	0.366	0.34	1.412	0.272
0.46	1.422	0.204	0.45	1.228	0.181	0.21	1.470	0.387	0.31	1.368	0.275
0.42	1.358	0.209	0.41	1.157	0.192	0.18	1.373	0.409	0.27	1.349	0.295
0.38	1.276	0.228	0.37	1.096	0.196	0.16	1.298	0.423	0.23	1.343	0.356
0.35	1.203	0.237	0.33	1.020	0.202	0.14	1.235	0.433	0.19	1.265	0.391
0.31	1.142	0.247	0.30	0.958	0.206	0.12	1.172	0.454	0.17	1.225	0.400
0.28	1.053	0.254	0.27	0.900	0.221	0.10	1.010	0.490	0.16	1.154	0.428
0.24	0.970	0.266	0.24	0.834	0.234	0.05	0.903	0.590	0.14	1.099	0.446
0.18	0.911	0.291	0.18	0.724	0.266	–	–	–	0.12	1.022	0.470
0.10	0.772	0.418	0.10	0.653	0.374	–	–	–	0.10	0.967	0.496
0.05	0.626	0.510	0.05	0.504	0.485	–	–	–	0.05	0.775	0.593

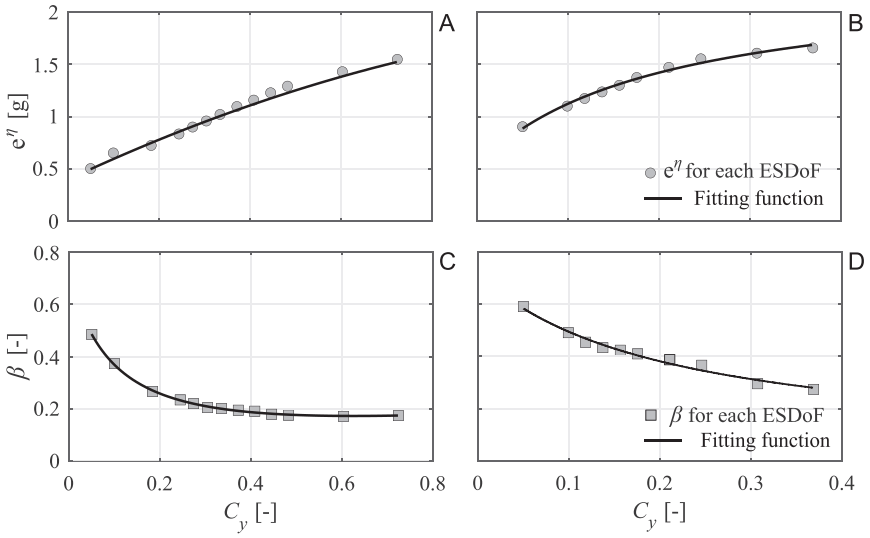

FIGURE 7 Fitting of continuous curves for the fragility parameters of the generated ESDoF oscillators against C_y: (A) curve for e^{η}, three-storey building, Y direction; (B) curve for e^{η}, six-storey building, X direction; (C) curve for β, three-storey building, Y direction; (D) curve for β, six-storey building, X direction

The figure shows that median capacity e^{η} increases with increased yield strength of the structure, as expected. On the other hand, the dispersion appears to be higher for the weaker variants of each building type with respect to the more resistant ones; in other words, β is higher at lower yield strength coefficients. This can be explained by the fact that T^* increases with decreasing C_y. While it is convenient to maintain the same IM for all structures considered, at the lower end of C_y the period T^* tends to approach the upper bound of the period interval behind the definition of Sa_{avg}; it is therefore to be expected that the IM exhibit lower efficiency for those structures.

2.7 | Benchmark sites and hazard curves

For the purposes of this study, ten benchmark Italian sites were considered and seismic hazard curves were computed via PSHA, with the aid of the software REASSESS.[39] These hazard curves provide $\lambda_{sa_{avg}}$ for each site, that is the annual rate of earthquakes exceeding any threshold of average spectral acceleration sa_{avg}, as defined in Equation (8).

It is important to highlight that the seismic source model[40] used in PSHA is the same as the one underlying the code's seismic design actions. This means that the failure rates from the risk analysis that will follow, and the exceedance rates of design actions are comparable, because they stem from the same model. Furthermore, the seventeen vibration periods

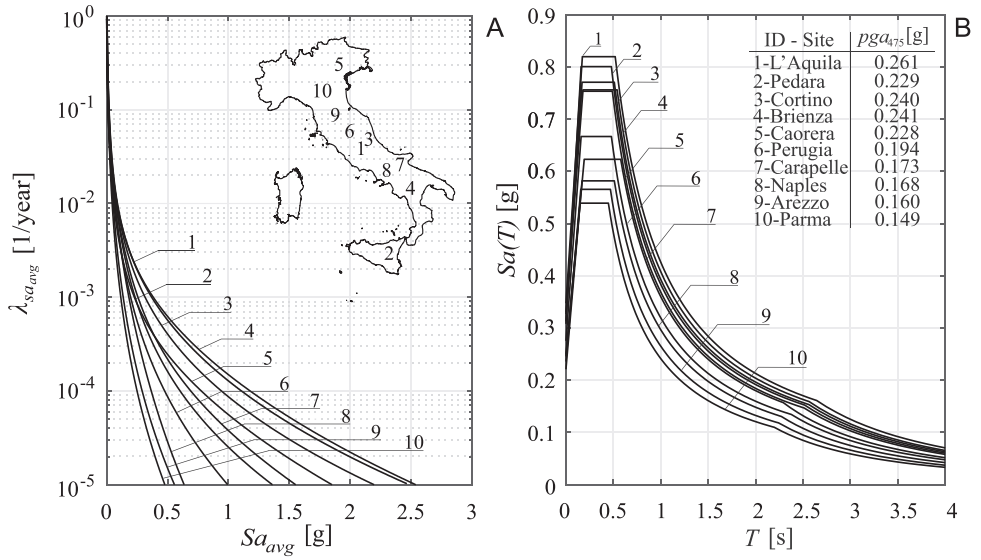

FIGURE 8 (A) Hazard curves in terms of Sa_{avg} for the case-study sites; (B) 475-year-return-period horizontal elastic (uniform-hazard) spectra according to NTC18

used to define Sa_{avg}were chosen so that model parameters were directly obtainable from the ground motion prediction equation that was used in the PSHA, in combination with a correlation model for the spectral ordinates.[41]

The location of the considered sites and the corresponding hazard curves are shown in Figure 8, along with their peak ground acceleration (PGA) value of the design spectra for $T_R = 475$ years, denoted as pga_{475} (hereafter roughly considered as a proxy of each site's design-level hazard), and with the respective site-specific 475 year return period elastic design spectrum for ground type C, according to EC8 classification (which is the same as the Italian code's). Note that the sites are numbered from one to ten in descending order of pga_{475}; however, it is evident from the figure that this order is not preserved by Sa_{avg} at longer return periods, as the corresponding hazard curves can be seen to intersect. In addition to the numbering labels, the figure also reports the name of the corresponding administrative municipality for the sake of context.

3 | RESULTS AND DISCUSSION

3.1 | Assigning behavior factors to the ESDoF systems

The set of ESDoF oscillators, representing incarnations of the reference structural configurations, differing only in their levels of lateral strength, can be ideally placed in any of the benchmark sites under consideration, that is assuming that each one's yield strength coefficient is the result of a different behavior factor that has been applied to that site's elastic design spectrum. In other words, it is assumed that each ESDoF system of given C_y, could have been the outcome of a seismic design at any of the benchmark sites using a free choice of q factor, disregarding for the moment the code-mandated $q_{\max}$. Essentially, this exercise entails assigning a different q factor per reference structural configuration, C_y and site. This operation must account for overstrength, which can be quantified via two factors that are respectively denoted in EC8 as α_1 and α_u, and defined by Equation (9):

$$\begin{cases} \alpha_1 = V_{yield}/V_d \\ \alpha_u = V_{\max}/V_d \end{cases}. \tag{9}$$

Factor α_1 is larger than unity because, at section-level design, material partial safety factors are used and nominal strength demand can be exceeded due to practical detailing considerations, while α_u mainly depends on the redundancy of the structural system and preferential mobilization of ductile over brittle local failure mechanisms due to capacity design.

TABLE 5 Overstrength factors from the SPOs of the case-study structures

Site	three-storey, X direction			three-storey, Y direction			six-storey, X direction			six-storey, Y direction		
	$V_e/V_{\max}$ [-]	α_u [-]	α_1 [-]	$V_e/V_{\max}$ [-]	α_u [-]	α_1 [-]	$V_e/V_{\max}$ [-]	α_u [-]	α_1 [-]	$V_e/V_{\max}$ [-]	α_u [-]	α_1 [-]
L'Aquila	1.40	2.78	1.37	1.51	2.60	1.52	1.72	2.28	1.30	1.40	2.79	1.22
Naples	1.37	2.84	1.58	1.29	3.00	1.46	1.70	2.29	1.17	1.69	2.31	1.24
Milan	<1	9.26	3.81	<1	8.34	3.43	<1	8.85	3.78	<1	8.18	3.51

TABLE 6 Minimum realistic yield strength coefficient $C_y^{\min}$ considered

	three-storey, X direction	three-storey, Y direction	six-storey, X direction	six-storey, Y direction
$C_y^{\min}$ [-]	0.24	0.24	0.10	0.12

Before proceeding any further, two considerations must be made. The first emerges directly from observing Figure 3C, showing pushover curves of the structures designed for Milan, which is characterized by the lowest seismic hazard among the three sites of the original (reference) designs (the other two being, Naples, and L'Aquila). From the figure it can be surmised that, due to the design base shear V_d for that site being so low, the actual lateral resistance $V_{\max}$ is no longer determined by V_d and typical overstrength due to redundancy and material partial safety factors. In fact, $V_{\max}$ is determined by other design requirements, such as the intrinsic lateral resistance of frames proportioned by gravity-load design and minimum design provisions for the geometry and reinforcement of structural members. This can be seen in Table 5, which shows the α_1 and $\alpha_u$overstrength ratios and the ratio of unmitigated elastic demand to lateral strength, $V_e/V_{\max}$, for all reference structures. In fact, the latter drops just about below unity for the Milan buildings, meaning that no arbitrary reduction of the q factor would have led $V_{\max}$ to be governed by seismic design.

Based on this observation, the reference buildings designed for the site in Milan are considered to exhibit a minimum value of the yield strength coefficient, $C_y^{\min}$, which cannot be undercut by reducing elastic seismic design forces. In other words, structures with yield strength coefficient lower than $C_y^{\min}$, whose values are reported in Table 6, would fail to meet various non-seismic functionality and safety requirements. Therefore, values of $C_y < C_y^{\min}$ are only considered in the following for completeness of the investigation, all the while being aware that structures weaker than that are unlikely to result from engineer design.

The second consideration emanates from Equation (4), which reflects the fact that the elastic spectral acceleration demand $Sa(T_1)$ is read off the code spectrum at the first-mode period from modal analysis of the numerical model assembled for design purposes. As mentioned previously, this period is different than T^*, which corresponds to the secant stiffness at nominal yield assigned to the ESDoF oscillators and, while T_1 is known for the reference structures that were actually the object of design, this is not so for the ESDoF systems generated by interpolating between the reference backbones. For this reason, a design-model period T_1 was assigned to each ESDoF oscillator, by interpolating between the ratios $T_1/T^*$of the reference structures. These values are shown in Table 7 for each of the two structural configurations and principal directions.

With these considerations in mind, the behavior factor to be allotted to each ESDoF system placed at each one of the benchmark sites, is given by Equation (10):

$$q = \frac{V_e}{V_d} = \frac{m^* \cdot Sa\,(T_1)}{F_c^*} \cdot \alpha_u, \tag{10}$$

where $Sa(T_1)$ is taken from each benchmark site's elastic spectrum in Figure 8, and there is the implicit assumption that $V_{\max} \approx \Gamma \cdot F_c^*$, in other words, that the maximum base shear corresponding to each backbone can be obtained from the capping-point resisting force multiplied by Γ. For this calculation, the modal participation factor value $\Gamma = 1.3$ is assumed for all ESDoF systems, a simplification that can be justified by the fact that Γ values obtained for the structures with available numerical models varied from 1.26 to 1.33. Furthermore, a overstrength ratio α_u had to be assigned to each ESDoF oscillator's backbone. The overstrength factors are assigned by assuming a constant value for $\alpha_1 = 1.3$, which is rounded down from 1.36, that being the average of the α_1 ratios obtained from the SPOs of the reference structures designed for L'Aquila and Naples, and by interpolating the ratio α_u/α_1 between reference structures. This is intended to reflect the

TABLE 7 Design model first-mode periods T_1 assigned to the generated ESDoF systems

three-storey, X direction		three-storey, Y direction		six-storey, X direction		six-storey, Y direction	
C_y [-]	T_1 [s]	C_y [-]	T_1 [s]	C_y [-]	T_1 [s]	C_y [-]	T_1 [s]
0.74	0.37	0.72	0.38	0.37	0.73	0.52	0.65
0.62	0.41	0.60	0.41	0.31	0.80	0.43	0.71
0.49	0.44	0.48	0.46	0.25	0.90	0.34	0.79
0.46	0.47	0.45	0.49	0.21	0.88	0.31	0.77
0.42	0.50	0.41	0.53	0.18	0.88	0.27	0.76
0.38	0.53	0.37	0.57	0.16	0.99	0.23	0.77
0.35	0.57	0.33	0.63	0.14	1.14	0.19	0.80
0.31	0.62	0.30	0.66	0.12	1.35	0.17	0.90
0.28	0.72	0.27	0.70	0.10	1.66	0.16	1.02
0.24	0.86	0.24	0.74	0.05	2.34	0.14	1.19
0.18	0.99	0.18	0.85	–	–	0.12	1.42
0.10	1.34	0.10	1.16	–	–	0.10	1.55
0.05	1.90	0.05	1.63	–	–	0.05	2.19

fact that the overstrength ratio α_1 depends on material partial safety factors applied at section-level flexural design and on provided reinforcement overshooting the nominal requirement; it can therefore be considered invariant among the different-strength incarnations of a structure.

The q factors assigned to each ESDoF oscillator at each benchmark site, are plotted in Figure 9, where continuous q -C_y curves have been fitted to the single values. Details on the analytical form of the curves and corresponding least-squares fitting can be found in an electronic supplement available at http://wpage.unina.it/iuniervo/papers/q-factor_supplement.pdf. The figure also delineates $C_y^{\min}$ considered for each structural configuration, so that the part of the curve to the left of the dashed line represents cases of low lateral strength that are only theoretical and are not expected to correspond to modern code-conforming structures.

3.2 | Risk-targeted q factors

Having obtained fragility parameters as a function of C_y and hazard curves at each benchmark site, the failure rate λ_f can be calculated for any combination of an ESDoF system's presumed design location and lateral strength, according to Equation (1). As a first step, λ_f was calculated for the structures having a yield strength coefficient that corresponds to design under $q = 3.9$, denoted as $C_y^{q=3.9}$, this being the behavior factor used for design of the reference structures. The results of this exercise are provided in Table 8.

The failure rates listed in the table confirm a fact that was already highlighted by past research,[4–8] that structures designed with the same behavior factor, applied to design spectra of the same T_R at different sites, exhibit different levels of seismic risk. One worthwhile observation is that, while the sites are ordered in terms of descending pga_{475}, and the yield strength coefficients duly follow suit, the failure rates do not follow a strictly descending order. As will be discussed later, this is also consequence of the different shapes of each site's hazard curve beyond the design return period intensity, which are evident in Figure 8A. Even so, the difference in λ_f, between the site with the highest risk in the list (no.4 Brienza) and the lowest (no.10 Parma), is almost two orders of magnitude.

The same procedure as above was implemented for all four structural configurations, values of C_y and benchmark sites. The results of this operation are provided in Figure 10, which plots failure rate against yield strength coefficient as a continuous curve for each benchmark site and structural configuration. Also in this plot, each panel is divided in two by a vertical line corresponding to $C_y^{\min}$, so that portions of the curves to the left of the dashed lines are assumed non-applicable for modern code-conforming structures.

According to the discussion of the previous paragraph, a q factor that would have ostensibly led to each C_y value via design has been assigned for all ESDoF systems and benchmark sites. Thus, by replacing all C_y values in the plots of Figure 10 with their counterpart q factors shown in Figure 9, a new set of curves was obtained, shown in Figure 11, providing

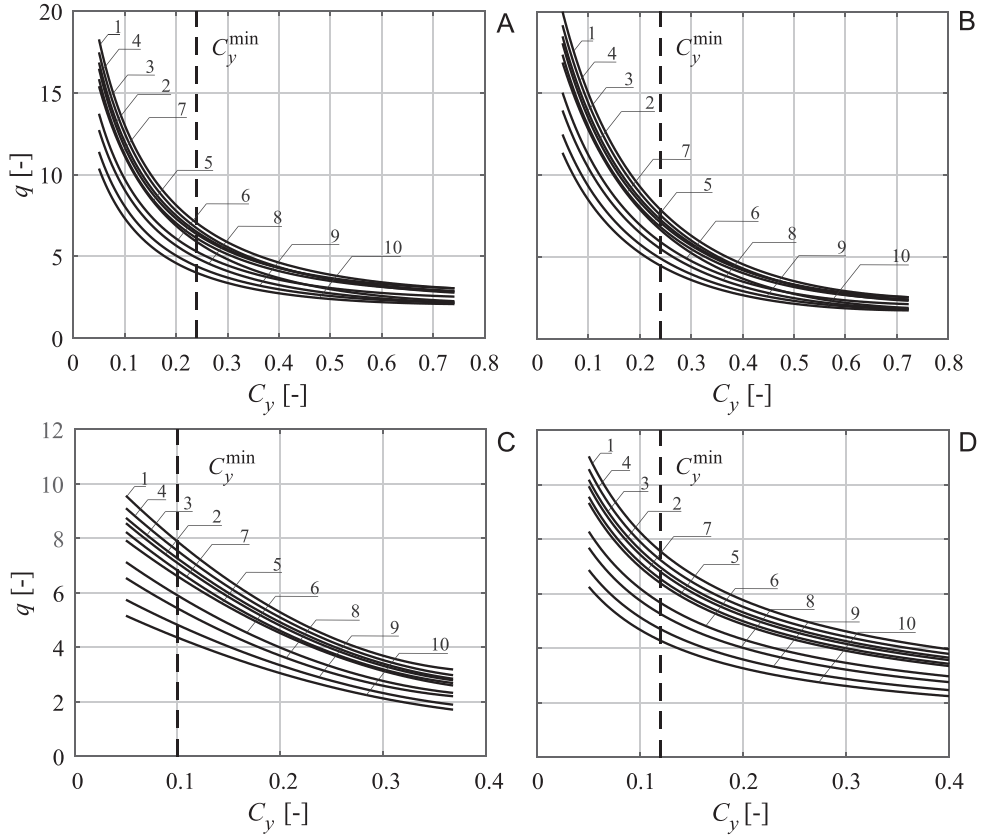

FIGURE 9 Continuous fitted curves of q factor against yield strength coefficient C_y for each site and type of structure: (A) three-storey building, X direction; (B) three-storey building, Y direction; (C) three-storey building, Y direction; (D) six-storey building, Y direction

TABLE 8 Failure rates of the SDoF oscillators corresponding to q factor equal to 3.90 at each site

ID - Site	three-storey, X direction		three-storey, Y direction		six-storey, X direction		six-storey, Y direction	
	$C_y^{q=3.9}$ [-]	λ_f [10^{-5}/year]	$C_y^{q=3.9}$ [-]	λ_f [10^{-5}/year]	$C_y^{q=3.9}$ [-]	λ_f [10^{-5}/year]	$C_y^{q=3.9}$ [-]	λ_f [10^{-5}/year]
1 – L'Aquila	0.50	5.52	0.46	9.14	0.28	5.51	0.41	5.04
2 – Pedara	0.46	1.10	0.43	1.93	0.25	1.16	0.34	1.14
3 – Cortino	0.45	4.25	0.43	6.76	0.26	4.06	0.35	4.02
4 – Brienza	0.45	7.30	0.43	11.40	0.27	6.67	0.38	6.40
5 – Caorera	0.43	2.93	0.41	4.60	0.24	2.76	0.31	2.88
6 – Perugia	0.36	0.63	0.36	1.03	0.21	0.62	0.24	0.71
7 – Carapelle	0.38	2.31	0.38	3.48	0.24	1.87	0.30	1.98
8 – Naples	0.32	0.10	0.33	0.18	0.19	0.13	0.21	0.16
9 – Arezzo	0.28	0.11	0.30	0.16	0.16	0.12	0.17	0.17
10 – Parma	0.25	0.07	0.28	0.10	0.13	0.10	0.14	0.14

failure rates and associated behavior factors for each benchmark site and structural configuration. In this new mapping of failure rate against q factor, the delimitation becomes slanted but remains approximately linear, dividing each plot of Figure 11 into two regions shown with different shading; in this case, the shaded regions to the right correspond to the domain where lateral strength is likely determined by design requirements unrelated to the behavior factor, according to the assumptions presented in the previous paragraphs. The figure gives a broader picture of what was already observed in the failure rate values of Table 8: seismic risk as a function of behavior factor differs from one site to another and, while risk is generally higher at sites under higher seismic hazard, the ranking order of the risk curves deviates from that of

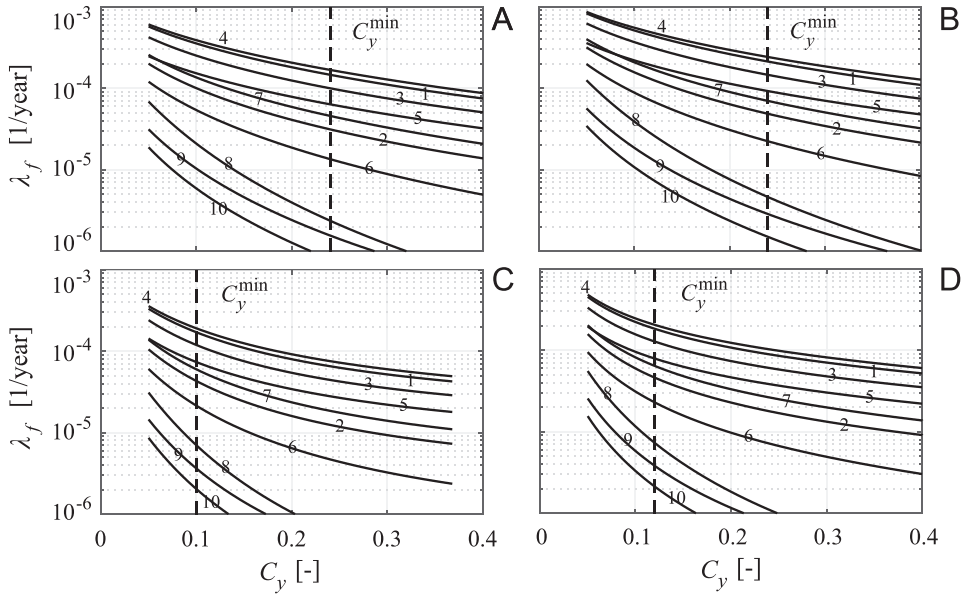

FIGURE 10 Failure rate against yield strength coefficient curves for (A) three-storey building, X direction; (B) three-storey building, Y direction; (C) six-storey building, X direction; (d) six-storey building, Y direction

TABLE 9 Risk-targeted q factor for the case-study sites with different seismic hazard level

q_R [-]				
ID - Site	**three-storey, X direction**	**three-storey, Y direction**	**six-storey, X direction**	**six-storey, Y direction**
4 - Brienza	4.74	3.48	5.43	4.93
1 – L'Aquila	5.51	4.22	6.15	5.56
3 – Cortino	6.52	5.39	6.83	6.21
5 – Caorera	(8.35)	(7.31)	(7.56)	(7.32)
7 – Carapelle	(9.40)	(8.50)	(7.49)	(7.53)
2 – Pedara	(11.67)	(10.83)	(8.49)	(8.78)
6 – Perugia	(12.80)	(11.80)	–	–
8 - Naples	–	(13.28)	–	–

elastic demand in terms of force. This can be attributed to the fact that risk depends on the shape of the hazard curve well beyond the design intensity as will be discussed in the following paragraphs.

At this point, an arbitrary risk target is assumed for λ_f, equal to 10^{-4} events/year,[8,42] uniform across all benchmark sites. Thus, for each benchmark site and structural configuration, a risk-targeted behavior factor, q_R, can be estimated by finding the intersection of the $\lambda_f = 10^{-4}$ horizontal line with each curve in Figure 11. The risk-targeted behavior factors corresponding to the assumed risk target, are given in Table 9, where the q_R values are shown in parentheses whenever the intersection of the target risk line and the curve falls within the shaded area, indicating that the lateral strength level required would likely be overridden by non-seismic design requirements. In the table, dashes appear whenever no q_R value could be obtained due to lack of intersection of the curves in Figure 11 with the risk target line. Obtaining an intersection for those cases, which comprise all structures at sites no. 9 and 10, would entail considering SDoF systems with $C_y < 0.05$, which was ruled out. The q_R values are also given in Figure 12, where they are plotted against the elastic spectral acceleration demand $Sa(T_1)$ of each benchmark site, marked with a grey circle when the corresponding yield strength coefficient is below $C_y^{\min}$ and a black circle otherwise. The figure shows the general trend of decreasing risk-targeted behavior factors with increasing hazard, the latter expressed in terms of the code's nominal 475 year T_R spectral ordinate, which is nevertheless not perfectly monotonic.

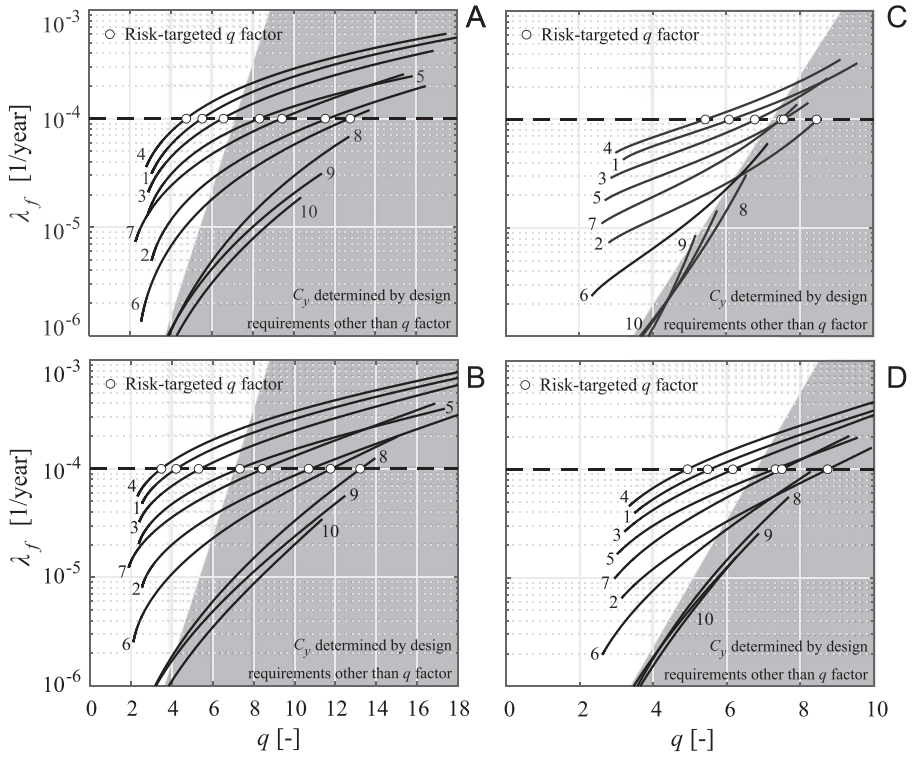

FIGURE 11 Curves providing the variation of λ_f as a function of q factor per benchmark site for (A) the three-storey building in the X direction; (B) the three-storey building in the Y direction; (C) the six-storey building in the X direction; (D) the six-storey building in the Y direction

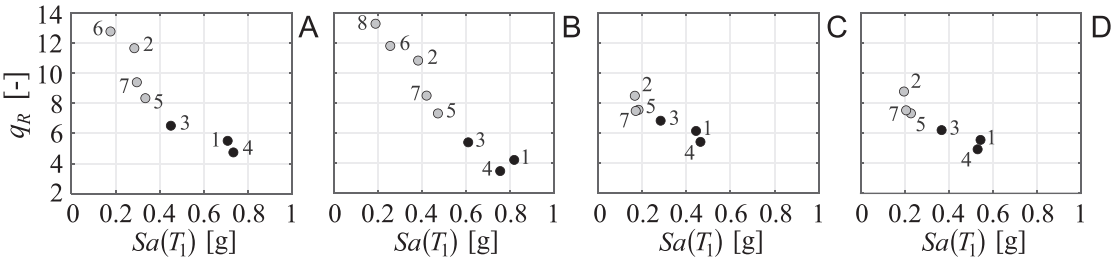

FIGURE 12 Scatter plots of the risk-targeted behavior factors against the code's elastic spectral ordinate for (A) the three-storey building, X direction; (B) the three-storey building, Y direction; (C) the six-storey building, X direction; (D) the six-storey building, Y direction

The yield strength coefficients corresponding to the risk-targeted behavior factor at each site, C_y^R, as well as the corresponding fragility parameters, η_R and β_R are reported in Table 10. Yield strength coefficients that fall below the assumed $C_y^{\min}$ are reported in parentheses.

3.3 | Evaluation of the results

As a general preamble to the discussion of these results, it should be noted that, due to both the performance threshold and target risk being arbitrary, the q_R values shown in the Table 9 are intended for comparison with one another, and not with the $q_{\max}$ value adopted for the design of the original reference structures. In this light, there are two observations to make. The first is that there is some variation of the risk-targeted behavior factor even for structures that are located at the same site and share the same type of lateral-load resisting system but differ in actual layout of structural elements in plan or in the number of storeys. The second observation is that harmonization of risk across different sites, via calibration of the q factor, only appears to be possible among sites characterized by higher seismic hazard, since the lateral resistance levels

TABLE 10 Risk-targeted yield strength coefficient and fragility parameters per structural configuration and sites

ID-Site	three-storey, X direction			three-storey, Y direction			six-storey, X direction			six-storey, Y direction		
	C_y^R [-]	e^{η_R} [g]	β_R [-]	C_y^R [-]	e^{η_R} [g]	β_R [-]	C_y^R [-]	e^{η_R} [g]	β_R [-]	C_y^R [-]	e^{η_R} [g]	β_R [-]
4 – Brienza	0.36	1.24	0.23	0.48	1.22	0.18	0.18	1.38	0.40	0.25	1.32	0.33
1 – L'Aquila	0.32	1.17	0.24	0.43	1.15	0.18	0.16	1.33	0.42	0.21	1.27	0.36
3 – Cortino	0.24	1.02	0.27	0.32	0.98	0.20	0.12	1.18	0.47	0.15	1.14	0.43
5 – Caorera	(0.16)	0.86	0.33	(0.22)	0.82	0.24	(0.07)	1.00	0.54	(0.10)	0.98	0.51
7 – Carapelle	(0.13)	0.80	0.36	(0.18)	0.75	0.27	(0.07)	0.97	0.55	(0.09)	0.94	0.52
2 – Pedara	(0.10)	0.73	0.40	(0.14)	0.68	0.31	(0.05)	0.90	0.58	(0.07)	0.87	0.56
6 – Perugia	(0.06)	0.64	0.49	(0.09)	0.58	0.39	–	–	–	–	–	–
8 – Naples	–	–	–	(0.06)	0.51	0.46	–	–	–	–	–	–

required to render risk at lower-hazard sites equal to that of the higher ones, appears to be unrealistically low. In fact, as can be seen in Figure 11, even if the arbitrary risk target assumed for the example were to be lowered, the curves of some of the benchmark sites would continue to be intersected by the horizontal threshold line within the shaded area, indicating that it was not possible to achieve the uniform risk objective set forth for that benchmark site, without resorting to yield strength coefficients that are unacceptably low for code-conforming engineered structures. This lower bound of lateral strength is attributed to two factors: first, cross section dimensions and flexural reinforcement are designed in compliance with minimum code-mandated values, independently of the severity of design seismic actions. Second, the redundancy that is typical of cast-in-situ moment-resisting RC frames, means that even if the latter were designed exclusively for gravity loads, they would still exhibit some level of lateral force resistance that is independent of any behavior factor applied to seismic actions.

A tempting way to sum-up this fact, could be to say that it is not possible to achieve the same level of seismic risk between high- and low-hazard sites via q factors. However, this qualitative distinction between high- and low-hazard sites is hard to make based, for example, on the PGA of the code's elastic spectrum at typical design return periods. A comparison between Figure 8 and Figure 11 reveals that the order of the $\lambda_f - q$ curves also depends on the shape of the hazard curves, mainly at return periods higher than the ones considered for design, which is not unexpected according to previous studies.[43]

Herein, *disaggregation* of structure-specific seismic risk is used to take a closer look at this effect. Disaggregation of the failure rate is calculated according to Equation (11):

$$f_{IM|f}\,(im) = \frac{P\,[f|IM = im]}{\lambda_f} \cdot \left|\frac{d\lambda_{im}}{\mathrm{dim}}\right|, \tag{11}$$

where $f_{IM|f}(im)$ is the conditional density of the shaking intensity given that structural failure has occurred. This operation was performed for two ESDoF systems, corresponding to the Y direction of the three-storey building and the X-direction of the six-storey building, each under two assumptions for the behavior factor, namely the risk-targeted q_R from Table 9 or $q = 3.9$, and at three benchmark sites, namely Brienza, Caorera and Pedara. The resulting plots are given in Figure 13, where risk disaggregation of the $q = 3.9$ structures is shown in black and that of the q_R structures in grey (small irregularities visible in the disaggregation curves are due to numerical issues).

On the same plots, the median capacities corresponding to the two choices of q factor, η_R and $\eta_{q=3.9}$, are indicated by vertical dashed lines and so is the average spectral acceleration value with $T_R = 475$ years, $sa_{avg,475}$.

Broadly speaking, the risk disaggregation shown in the figure can be interpreted as indicative of the shaking intensity that will be most likely causative of an observed failure of the structure at the given site. Figure 13A shows the case of the three-storey building's Y direction at Brienza, where passing from $\lambda_f = 1.14 \cdot 10^{-4}$ events/year for $q = 3.9$ to the (arbitrary) target of $\lambda_f = 10^{-4}$ events/year required an adjustment to $q \approx 3.5$. In all other cases, achieving this specific level of uniform risk entailed shifting median capacity to the left of that corresponding to $q = 3.9$ by increasing the behavior factors to achieve lower lateral strength. Therefore, the transition to uniform risk was achieved by altering structural capacity, so that different segments of the site-specific hazard curve become relevant in determining the failure rate.

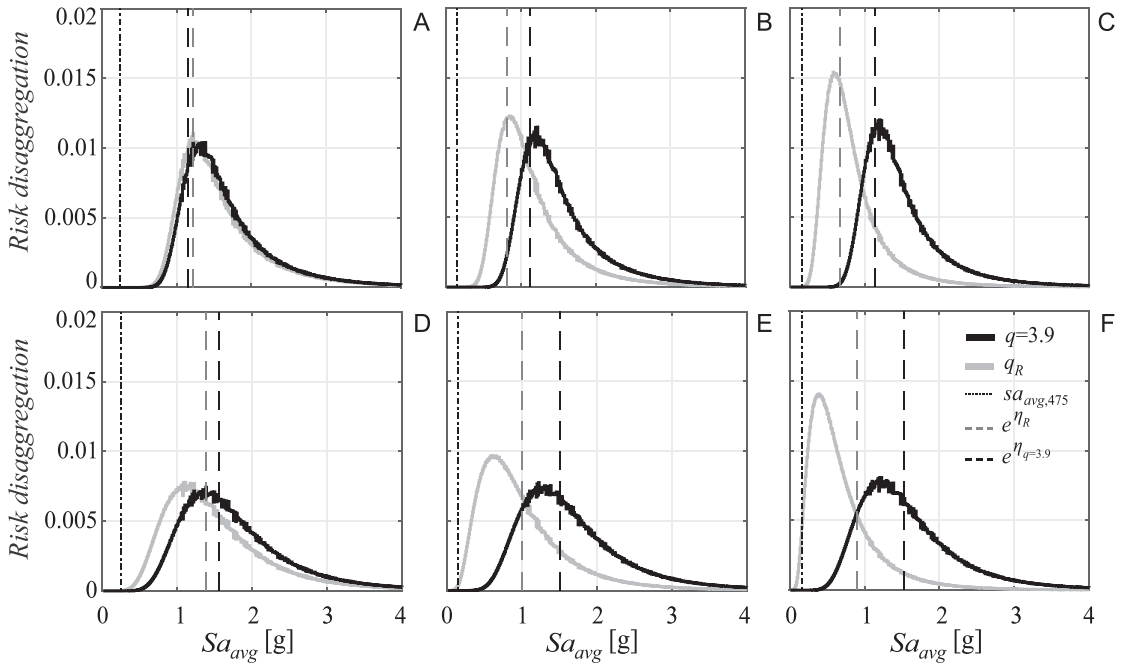

FIGURE 13 Risk disaggregation for ESDoF oscillators corresponding to uniform q and uniform risk, corresponding to the three-storey building in the Y direction at (A) Brienza, (B) Caorera, (C) Pedara, and the six-storey building in the X direction at (D) Brienza, (E) Caorera, (F) Pedara

Additionally, it is important to highlight that, in all cases, failure to meet this specific performance objective will most likely be caused by intensities larger than the one corresponding to the return period of the design seismic actions. This explains the fact that, when the same behavior factor is used across all sites, the failure rates do not always rank under an order that can be explained by the ranking of design spectral ordinates at $T_R = 475$ years: as can be seen from Figure 8, the hazard curves beyond the design return period differ in shape and may even intersect, but it is that part of the curves that mostly influences precedence in terms of risk. As a result, the trend of q_R against said spectral ordinates shown in Figure 12 is neither regular, nor monotonic. A clear example of this comes from comparing the results for sites no.4 (Brienza) and no.5 (Caorera): passing from a site with a pga_{475} of 0.24 g to one of 0.23 g, the q factor needed for maintaining the arbitrary common risk level shoots from approximately 3.5 to 7.3. This is because risk associated with large displacement demands is more likely to be determined by seismic actions of larger return periods and the PGA value of the design spectrum cannot account for those.

For the cases examined here, it was shown that there is leeway for obtaining uniform levels of seismic safety by adjusting the q factor only between sites characterized by *higher* hazard levels. Figure 11 shows that, for each structure and site, the point where the failure rate-behavior factor curve breaks into the shaded area corresponds to a *maximum* value of λ_f, that cannot be superseded by further increase of the q factor, for the reasons described above. This implies that this point corresponds to a *minimum* level of seismic safety that the structure will exhibit when designed under any q factor to the right of the demarcation line, since lateral resistance past that point should become insensitive to the reduction of seismic design actions. Thus, although it appears that uniform seismic safety cannot always be achieved between all sites by adjusting the behavior factor, one could acquiesce to q factors that allow structures to exhibit the same risk across high-hazard sites while remaining below a certain risk threshold at low-hazard sites, which can be possibly defined as acceptable according to some criterion.[44] However, as already discussed, what constitutes a high-hazard or a low-hazard site, in this context, is by no means obvious from the elastic design spectrum alone.

4 | CONCLUSIONS

The present study investigated the question of whether it is practical to achieve uniform levels of seismic safety for code-conforming structures designed at different sites, using force-based design and behavior factors. To address this issue,

seismic risk calculations for several case-study reinforced concrete structures were developed. In these risk calculations a single performance objective was considered, one that entails entry of the structures in the inelastic range, and the only source of uncertainty considered was that due to record-to-record variability of structural response. Another simplification lies in the fact that only bare frames were considered and the potential influence of infill walls in the response was neglected.

Two main results emerged from this investigation. The first result was that, at some of the sites considered, the behavior factors that would have supposedly led to uniform risk among all sites, are too large to be applicable in practice. The reason for this is that code-mandated detailing requirements and gravity-load design should provide a minimum level of lateral strength that is insensitive to risk-targeted fluctuations of the behavior factor. Although this issue has also emerged in past research, the present investigation additionally highlighted the fact that the dividing line between high-hazard sites, where uniformity of seismic risk via appropriately calibrated q factors is applicable, and low-hazard sites, where it is not, cannot be defined based on the code's elastic design spectrum. The reason behind this, is that the distinction is decided by the shape of the hazard curve beyond the return period of the design actions. This was highlighted by one case where a five percent decrease in the design spectrum's peak ground acceleration when passing from one Italian site to another, was accompanied by more than doubling of the behavior factor required to maintain the same failure rate. Nevertheless, it should be pointed out that the non-applicability of uniform seismic safety via risk-targeted behavior factors at lower-hazard sites, stems from the fact that, at those sites, a minimum level of safety is implicitly guaranteed by design against other actions that cannot be reduced further by increasing q factors.

The second main result is that a risk-targeted behavior factor is structure- and site-specific to the point that a-priori definition in a normative document appears unfeasible. Although the present study considered a limited number of structures, the ones that it did consider stemmed from design of the same layout-in-plan of structural elements for different levels of seismic design actions. In other words, only the size of structural members and amount of reinforcing steel were allowed to vary between frames with the same number of storeys. Thus, not only were risk-targeted behavior factors of a given structure observed to vary from site to site, as expected from similar past research, but the same was true for the behavior factors of similar structures at a given site. This implies that the definition of such risk-targeted q factors can only be undertaken when the analyst is armed with information about the structure that is only available after design, which hints at an iterative procedure being more realistic than a-priori definition by the code.

ACKNOWLEDGEMENTS

This study was developed within the activities of the ReLUIS-DPC 2019–2021 research program, funded by *Presidenza del Consiglio dei Ministri – Dipartimento della Protezione Civile*, with the disclaimer that the opinions and conclusions presented herein are those of the authors and are not necessarily shared by the funding organization. The authors wish to express their gratitude to the RINTC project research group, whose results were instrumental in the development of the present study.

DATA AVAILABILITY STATEMENT

The data that supports the findings of this study are available in the supplementary material of this article.

ORCID

Georgios Baltzopoulos https://orcid.org/0000-0002-0460-6558
Iunio Iervolino https://orcid.org/0000-0002-4076-2718

REFERENCES

1. C.E.N. Eurocode 8: design of structures for earthquake resistance: part 1-1: general rules, seismic actions and rules for buildings. European Committee for Standardization; 2004.
2. CS.LL.PP. Norme tecniche per le costruzioni. *Gazz Uff della Repubb Ital*. 2018;42 (in Italian).
3. Žižmond J, Dolšek M. Evaluation of factors influencing the earthquake-resistant design of reinforced concrete frames according to Eurocode 8. *Struct Infrastruct Eng*. 2016;12(10):1323-1341. https://doi.org/10.1080/15732479.2015.1117112
4. Iervolino I, Spillatura A, Bazzurro P. Seismic reliability of code-conforming Italian buildings. *J Earthq Eng*. 2018;22(2):5-27. https://doi.org/10.1080/13632469.2018.1540372. sup.
5. Vamvatsikos D, Bakalis K, Kohrangi M, Pyrza S, Castiglioni CA, Kanyilmaz A, Morelli F, Stratan A, D' Aniello M, Calado L, Proença JM, Degee H, Hoffmeister B, Pinkawa M, Thanopoulos P, Vayas I. A risk-consistent approach to determine EN1998 behaviour factors for lateral load resisting systems. *Soil Dynamics and Earthquake Engineering*. 2020;131:106008. http://doi.org/10.1016/j.soildyn.2019.106008

6. Gkimprixis A, Tubaldi E, Douglas J. Comparison of methods to develop risk-targeted seismic design maps. *Bull Earthq Eng*. 2019;17(7):3727-3752. https://doi.org/10.1007/s10518-019-00629-w
7. Suzuki A, Baltzopoulos G, Iervolino I & RINTC-Workgroup A look at the seismic risk of Italian code-conforming RC buildings. In: 16th European Conference on Earthquake Engineering; 2018.
8. Žižmond J, Dolšek M. Formulation of risk-targeted seismic action for the force-based seismic design of structures. *Earthquake Engineering & Structural Dynamics*. 2019;48(12):1406–1428. http://doi.org/10.1002/eqe.3206
9. Costa A, Romão X, Oliveira CS. A methodology for the probabilistic assessment of behaviour factors. *Bull Earthq Eng*. 2010;8(1):47-64. https://doi.org/10.1007/s10518-009-9126-5
10. Yarahmadi H, Miri M, Rakhshanimehr M. A methodology to determine the response modification factor for probabilistic performance-based design. *Bull Earthq Eng*. 2017;15(4):1739-1769. https://doi.org/10.1007/s10518-016-0044-z
11. Suzuki A, Iervolino I. Seismic fragility of code-conforming Italian buildings based on SDoF approximation. *J Earthq Eng*. 1-35. https://doi.org/10.1080/13632469.2019.1657989. Published online 2019.
12. Vamvatsikos D, Cornell CA. Incremental dynamic analysis. *Earthq Eng Struct Dyn*. 2002;31(3):491-514. https://doi.org/10.1002/eqe.141
13. Cornell CA, Krawinkler H. Progress and challenges in seismic performance assessment. *PEER News*. 2000;3:1-3.
14. McGuire RK. *Seismic Hazard and Risk Analysis*. Earthquake Engineering Research Institute; 2004.
15. Cornell CA. Engineering seismic risk analysis. *Bulletin of the Seismological Society of America*. 1968;58(5):1583–1606. http://doi.org/10.1785/bssa0580051583
16. RINTC-Workgroup Results of the 2015–2017 Implicit Seismic Risk of Code-Conforming Structures in Italy, Final Report; 2018.
17. Ricci P, Manfredi V, Noto F, et al. Modeling and seismic response analysis of italian code-conforming reinforced concrete buildings. *J Earthq Eng*. 2018;22(sup2):105-139. https://doi.org/10.1080/13632469.2018.1527733
18. Ricci P, Di Domenico M & Verderame GM Parameters affecting the behaviour factor and the seismic safety of EC8-designed reinforced concrete buildings. In: COMPDYN 2019 - Proceedings of the 7th ECCOMAS Thematic Conference on Computational Methods in Structural Dynamics and Earthquake Engineering; 2019.
19. Fajfar P. A Nonlinear Analysis Method for Performance-Based Seismic Design. *Earthquake Spectra*. 2000;16(3):573–592. http://doi.org/10.1193/1.1586128
20. Baltzopoulos G, Baraschino R, Iervolino I, Vamvatsikos D. SPO2FRAG: software for seismic fragility assessment based on static pushover. *Bulletin of Earthquake Engineering*. 2017;15(10):4399–4425. http://doi.org/10.1007/s10518-017-0145-3
21. De Luca F, Vamvatsikos D, Iervolino I. Near-optimal piecewise linear fits of static pushover capacity curves for equivalent SDOF analysis. *Earthq Eng Struct Dyn*. 2013;42:523-543. https://doi.org/10.1002/eqe.2225
22. Priestley MJN. Performance based seismic design. *Bulletin of the New Zealand Society for Earthquake Engineering*. 2000;33(3):325–346. http://doi.org/10.5459/bnzsee.33.3.325-346
23. Aschheim M. Seismic Design Based on the Yield Displacement. *Earthquake Spectra*. 2002;18(4):581–600. http://doi.org/10.1193/1.1516754
24. Jalayer F, Cornell CA. *Direct Probabilistic Seismic Analysis: Implementing Non-Linear Dynamic Assessment*. Stanford University; 2003.
25. Vamvatsikos D, Cornell CA. Developing efficient scalar and vector intensity measures for IDA capacity estimation by incorporating elastic spectral shape information. *Earthq Eng Struct Dyn*. 2005;34(13):1573-1600. https://doi.org/10.1002/eqe.496
26. Bojórquez E, Iervolino I. Spectral shape proxies and nonlinear structural response. *Soil Dynamics and Earthquake Engineering*. 2011;31(7):996–1008. http://doi.org/10.1016/j.soildyn.2011.03.006
27. Baltzopoulos G, Baraschino R, Iervolino I. On the number of records for structural risk estimation in PBEE. *Earthq Eng Struct Dyn*. 2019;48(5):489-506. https://doi.org/10.1002/eqe.3145
28. Eads L, Miranda E, Lignos DG. Average spectral acceleration as an intensity measure for collapse risk assessment. *Earthq Eng Struct Dyn*. 2015;44(44):2057-2073. https://doi.org/10.1002/eqe.2575
29. Kazantzi AK, Vamvatsikos D. Intensity measure selection for vulnerability studies of building classes. *Earthq Eng Struct Dyn*. 2015;44:2677-2694. https://doi.org/10.1002/eqe.2603
30. Luco N, Cornell CA. Structure-Specific Scalar Intensity Measures for Near-Source and Ordinary Earthquake Ground Motions. *Earthquake Spectra*. 2007;23(2):357–392. http://doi.org/10.1193/1.2723158
31. Baltzopoulos G, Baraschino R, Iervolino I, Vamvatsikos D. Dynamic analysis of single-degree-of-freedom systems (DYANAS): a graphical user interface for OpenSees. *Eng Struct*. 2018;177:395-408. https://doi.org/10.1016/j.engstruct.2018.09.078. December.
32. McKenna F, Scott MH, Fenves GL. Nonlinear finite-element analysis software architecture using object composition. *J Comput Civ Eng*. 2010;24(1):95-107. https://doi.org/10.1061/(asce)cp.1943-5487.0000002
33. Ibarra LF, Medina RA, Krawinkler H. Hysteretic models that incorporate strength and stiffness deterioration. *Earthq Eng Struct Dyn*. 2005;34(12):1489-1511. https://doi.org/10.1002/eqe.495
34. FEMA Quantification of building seismic performance factors. Applied Technology Council, Federal Emergency Management Agency; 2008.
35. Baraschino R, Baltzopoulos G, Iervolino I. R2R-EU: Software for fragility fitting and evaluation of estimation uncertainty in seismic risk analysis. *Soil Dynamics and Earthquake Engineering*. 2020;132:106093. http://doi.org/10.1016/j.soildyn.2020.106093
36. Shome N, Cornell CA, Bazzurro P, Carballo JE. Earthquakes, Records, and Nonlinear Responses. *Earthquake Spectra*. 1998;14(3):469–500. http://doi.org/10.1193/1.1586011

37. Franchin P, Mollaioli F & Noto F RINTC project: influence of structure-related uncertainties on the risk of collapse of Italian code-conforming reinforced concrete buildings. In: COMPDYN 2017 - Proceedings of the 6th International Conference on Computational Methods in Structural Dynamics and Earthquake Engineering; 2017.
38. Iervolino I. Assessing uncertainty in estimation of seismic response for PBEE. *Earthq Eng Struct Dyn*. 2017;46(10):1711-1723. https://doi.org/10.1002/eqe.2883
39. Chioccarelli E, Cito P, Iervolino I, Giorgio M. REASSESS V2.0: software for single- and multi-site probabilistic seismic hazard analysis. *Bull Earthq Eng*. 2019;17(4):1769-1793. https://doi.org/10.1007/s10518-018-00531-x
40. Meletti C, Galadini F, Valensise G, et al. A seismic source zone model for the seismic hazard assessment of the Italian territory. *Tectonophysics*. 2008;450:85-108.
41. Jayaram N, Baker JW. Statistical tests of the joint distribution of spectral acceleration values. *Bull Seismol Soc Am*. 2008;98(5):2231-2243. https://doi.org/10.1785/0120070208
42. Tsang HH, Wenzel F. Setting structural safety requirement for controlling earthquake mortality risk. *Saf Sci*. 2016;86:174-183. https://doi.org/10.1016/j.ssci.2016.02.028
43. Iervolino I, Giorgio M, Cito P. The peak over the design threshold in strong earthquakes. *Bull Earthq Eng*. 2019;17(3):1145-1161. https://doi.org/10.1007/s10518-018-0503-9
44. Iervolino I, Pacifico A. Fatality rates implied by the Italian building code. *Earthquake Engineering & Structural Dynamics*. 2021;50(11):3083–3089. http://doi.org/10.1002/eqe.3472

How to cite this article: Baltzopoulos G, Grella A, Iervolino I. Seismic reliability implied by behavior-factor-based design. *Earthquake Engng Struct Dyn*. 2021;50:4076–4096. https://doi.org/10.1002/eqe.3546